

Sigmatropic rearrangements in 5-allyloxytetrazoles†

Luís M. T. Frija,^{‡a,b} Igor Reva,^{*b} Amin Ismael,^a Daniela V. Coelho,^a Rui Fausto^b and M. Lurdes S. Cristiano^{*a}

Received 22nd March 2011, Accepted 23rd May 2011

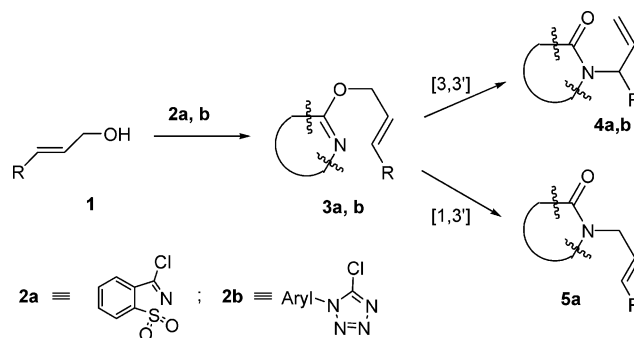
DOI: 10.1039/c1ob05460k

Mechanisms of thermal isomerization of allyl tetrazolyl ethers derived from the carbocyclic allylic alcohols cyclohex-2-enol and 3-methylcyclohex-2-enol and from the natural terpene alcohol nerol were investigated. In the process of the syntheses of the three 1-aryl-5-allyloxytetrazoles, their rapid isomerization to the corresponding 1-aryl-4-allyltetrazol-5-ones occurred. The experiments showed that the imidates rearrange exclusively through a [3,3']-sigmatropic migration of the allylic system from *O* to *N*, with inversion. Mechanistic proposals are based on product analysis and extensive quantum chemical calculations at the DFT(B3LYP) and MP2 levels, on *O*-allyl and *N*-allyl isomers and on putative transition state structures for [1,3']- and [3,3']-sigmatropic migrations. The experimental observations could be only explained on the basis of the MP2/6-31G(d,p) calculations that favoured the [3,3']-sigmatropic migrations, yielding lower energies both for the transition states and for the final isomerization products.

1. Introduction

Tetrazoles are applied in many areas, and these applications are often related to the acid/base properties and metabolic stability of the tetrazolic ring. Tetrazole¹ and its derivatives have important applications in medicinal chemistry, mainly as surrogates for carboxylic acids,²⁻⁷ in agriculture, as herbicides, fungicides and plant-growth regulators,⁸ in photography and photo-imaging, as stabilizers⁹ and in the car manufacturing industry, as gas-generating agents for airbags.¹⁰ Tetrazoles are also of use as multidentate nitrogen ligands¹¹ and are widely applied in synthesis.¹²⁻¹⁹ Tetrazolyl ethers are used as intermediate compounds for reductive cleavage of the C–O bond in phenols and alcohols. The strongly electron-withdrawing tetrazolyl system, together with oxygen from the original alcohol, represents an efficient nucleofuge in heterogeneous transfer hydrogenolysis catalyzed by transition metals.¹⁶⁻¹⁹ Aryl-, allyl-, benzyl-, and naphthyl-tetrazolyl ethers, used in this synthetic strategy, are easily obtained from reaction of the corresponding hydroxylic compound with commercially available 5-chloro-1-phenyl-(1*H*)-tetrazole.²⁰

The reactivity of benzisothiazolyl (saccharyl) and tetrazolyl derivatives of allyl alcohols (ethers **3a,b**; Scheme 1) was shown to be related to bond lengths around the central C_{HAR}–O–C_A ether



linkage (HAR = heteroaromatic ring and A = allyl), caused by the powerful electron-withdrawing effect of the saccharyl or tetrazolyl ring system.^{21,22} Upon etherification, the originally strong C_A–O bond in the allyl alcohol becomes weak, and the bond between the oxygen and the carbon of the heteroaromatic ring (C_{HAR}–O) becomes very strong. These electronic changes provide a molecular structure that lies close to a transition state structure in which the C_A–O bond in the ether becomes easily cleavable. Thus, ethers **3a,b** are readily converted into the corresponding *N*-allyl-isomers **4** or **5** when heated (Scheme 1).

An earlier investigation of the thermal rearrangement in 3-allyloxysaccharins **3a** (Scheme 1) in solution, revealed that migration of the allyl group from *O* to *N* may occur through both [3,3']- and [1,3']-processes,^{22,23} the relative proportion of products (**4a**, **5a**) depending on structural features of the starting ether such as electron density and steric hindrance on the allylic system, polarity of the reaction medium and temperature. It was demonstrated that, for compounds **3a**, the [3,3']-products undergo inversion to the thermochemically more favourable [1,3']-isomers upon extended

^aDepartment of Chemistry and Pharmacy, F.C.T. and CCMAR, University of Algarve, Campus de Gambelas, 8005-039 Faro, Portugal. E-mail: mcristi@ualg.pt; Fax: +351 289 800 066; Tel: +351 289 800 100 x 7642

^bDepartment of Chemistry, University of Coimbra, 3004-535 Coimbra, Portugal. E-mail: reva@qui.uc.pt; Fax: +351 239 827 703; Tel: +351 239 854 489

† Electronic supplementary information (ESI) available. See DOI: 10.1039/c1ob05460k

‡ Current address: iMed.UL, Faculdade de Farmácia da Universidade de Lisboa, Av. Prof. Gama Pinto, 1649-003 Lisboa, Portugal

heating.²³ It was also observed that the saccharyl derivative of the cyclic allyl alcohol myrtenol isomerises at ambient temperature with exclusive formation of the [1,3']-product. This behaviour was interpreted on the basis of steric constraints imposed by the cyclic myrtenyl system, which destabilize the transition state required for concerted [3,3']-migration, preventing its formation. For this derivative, the enthalpy of activation for the [3,3']-shift was calculated to be 67 kJ mol⁻¹ higher than that for the [1,3']-shift, thus explaining the observed selectivity.²² It is not clear whether the [1,3']-rearrangement in these ethers occurs through a fragmentation–recombination process or through a pseudo-pericyclic mechanism. Recently, the thermal isomerization of neat 3-allyloxysaccharin was investigated in the liquid phase, combining matrix-isolation FTIR spectroscopy, differential scanning calorimetry and quantum chemical calculations. From the results, a [3,3']-sigmatropic shift mechanism for the isomerization in the liquid phase was proposed.²⁴

Contrasting with the non-selective isomerization of 3-allyloxybenzothiazoles **3a**, kinetic studies have demonstrated that the thermal *O* to *N* migration of the allylic system in a range of 5-allyloxytetrazoles **3b** proceeds through a [3,3']-sigmatropic Claisen-type mechanism, with formation of isomers **4b**.^{22,25,26} The observed selectivity in the thermal isomerization of allyl tetrazolyl ethers has been advantageously used in the design of synthetic routes to other heterocycles. For instance, *N*-allyltetrazolones **4b** are quantitatively converted into 3,4-dihydro-pyrimidinones^{12,13,15} Therefore, due to the importance of this rearrangement reaction in synthesis, the structural effect of steric constraints imposed by bulky allylic moieties on selectivity should be properly explored. In particular, according to the best of our knowledge, there are no detailed studies of the isomerization of ethers **3b** using quantum chemical methods.

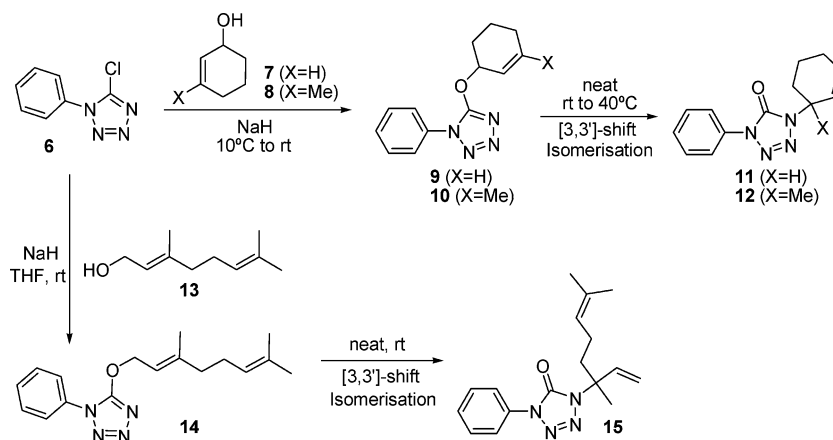
We now describe the results of our investigation on the sigmatropic isomerization of tetrazolyl ethers derived from the cyclic allyl alcohols cyclohex-2-enol (**7**) and 3-methylcyclohex-2-enol (**8**) and from the natural product nerol (**13**) (see Scheme 2). In the present investigation, ethers **9**, **10** and **14** were synthesised and thermally isomerised to the corresponding *N*-allyl isomers **11**, **12**, **15**, which were subsequently characterised. Extensive theoretical calculations (using the DFT(B3LYP)/6-31G(d,p) and MP2/6-31G(d,p) levels) were performed for ethers **9**, **10** and **14**, for the corresponding *N*-allyl isomers **11**, **12**, **15** resulting from a [3,3']-

sigmatropic shift of the allylic system (Scheme 2 and Fig. 1–4), for the corresponding *N*-allyl isomers **16–18** resulting from a [1,3']-sigmatropic shift of the allylic system (Scheme 2 and Fig. 1–4) and also for putative transition state structures **TS1a–TS3a** and **TS1b–TS3b**. Product analysis shows that the thermal isomerization of ethers **9**, **10** and **14** proceeds through an exclusive [3,3']-sigmatropic mechanism. Considering the results obtained from theoretical studies, the observed selectivity was ascribed to kinetic control.

2. Results and discussion

2.1 Synthesis and characterisation of tetrazolyl derivatives 9–12 and 14, 15

Allylic derivatives of tetrazole **9–12** and **14**, **15** were synthesised as depicted in Scheme 2. The carbocyclic allylic alcohols cyclohex-2-enol (**7**) and 3-methylcyclohex-2-enol (**8**) and the natural product nerol (**13**), were initially converted into the more nucleophilic allylic alkoxides, through reaction with sodium hydride in anhydrous conditions. Subsequent addition of 5-chloro-1-phenyltetrazole resulted in nucleophilic displacement of chloride, with formation of the required ethers **9**, **10** and **14**. Ether **9** could be isolated and characterised. However, putative ether **10** could not be isolated, as it readily isomerised to the corresponding tetrazolone **12**, under the conditions used for etherification. It was also observed that isomerization of ether **14** occurs very easily at room temperature. This ether was isolated as a solid (m.p. 43–45 °C), and the infrared spectrum registered immediately after isolation reveals the absence of bands corresponding to the carbonyl stretching vibration, indicating that no tetrazolone is detected. However the ¹H-NMR spectrum of the solid, obtained some days after isolation, clearly shows that ether **14** is already “contaminated” with its *N*-allyl isomer **15**. In ethers **10** and **14**, the allylic double bond is more substituted than in ether **9**. Assuming that the thermal sigmatropic isomerization occurs with development of a positive charge on the allylic moiety, the transition state structures obtained from **10** and **14** will be further stabilised, lowering the activation energy for isomerization. Thus, it is expected that the activation energy for thermal isomerization of ether **9** will be higher than that for ethers **10**, **14**. In fact, as stated, only ether **9** could be isolated. This ether was then heated to afford its neat *N*-allyl isomer **11**.



Scheme 2

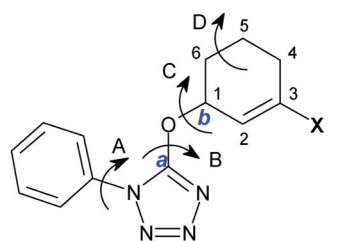
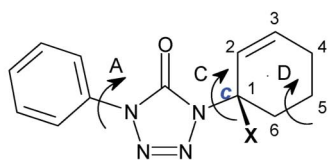
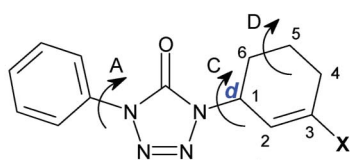
Ether [9 (X=H); 10 (X=CH₃)]Product of [3,3]-shift: 3,3'-tetrazolone [11 (X=H); 12(X=CH₃)]Product of [1,3]-shift: 1,3'-tetrazolone [16 (X=H); 17 (X=CH₃)]

Fig. 1 Top: Structure of allyl tetrazolyl ethers derived from the carbocyclic allylic alcohols: cyclohex-2-enol [5-(Cyclohex-2-enyloxy)-1-phenyl-1*H*-tetrazole (9) X = H] and 3-methylcyclohex-2-enol [5-(3-Methylcyclohex-2-enyloxy)-1-phenyl-1*H*-tetrazole (10) X = CH₃]. **Middle:** Structure of the rearrangement products resulting from [3,3]-sigmatropic migration of the allylic system: 1-(cyclohex-2-enyl)-4-phenyltetrazol-5-one (11) (X = H) and 1-(cyclohex-2-enyl)-1-methyl-4-phenyltetrazol-5-one (12) (X = CH₃). **Bottom:** Structure of the rearrangement products resulting from [1,3]-sigmatropic migration of the allylic system: 1-(cyclohex-2-enyl)-4-phenyltetrazol-5-one (16) (X = H) and 1-(3-methylcyclohex-2-enyl)-4-phenyltetrazol-5-one (17) (X = CH₃). Note that the X substituent remains attached to the same carbon atom during both sigmatropic migrations (though the formal atom numbering changes). The adopted atom numbering of the cyclohex-2-enyl ring is shown explicitly. Carbon atom C(1) of the cyclohex-2-enyl ring is chiral for all compounds. Arrows accompanied with letters A, B, C, D show intramolecular conformationally relevant degrees of freedom.

Analysis of the isomerization products by ¹H-NMR enables the differentiation between putative [1,3]- and [3,3]-products through analysis of the signals corresponding to resonances of protons of the allylic system, since resonances for these protons are predicted to be substantially different in inverted and non-inverted *N*-allyl isomers.

Concerning the isomerization of ether 10, the predicted ¹H-NMR spectra for putative rearranged products reveal, for the product of [1,3]-migration, compound 17, a characteristic signal at δ 4.06 (CH) for the allylic proton connected to the carbon that is linked to the tetrazolone ring and another characteristic signal at 5.37 (CH) for the sole vinyl proton (Table 1 and Fig. 2S, ESI[†]). However, for the product of [3,3]-migration, compound 12, an overlapping signal is predicted for the two vinyl protons, at δ 5.59 (CH). The experimental ¹H-NMR spectrum of the product

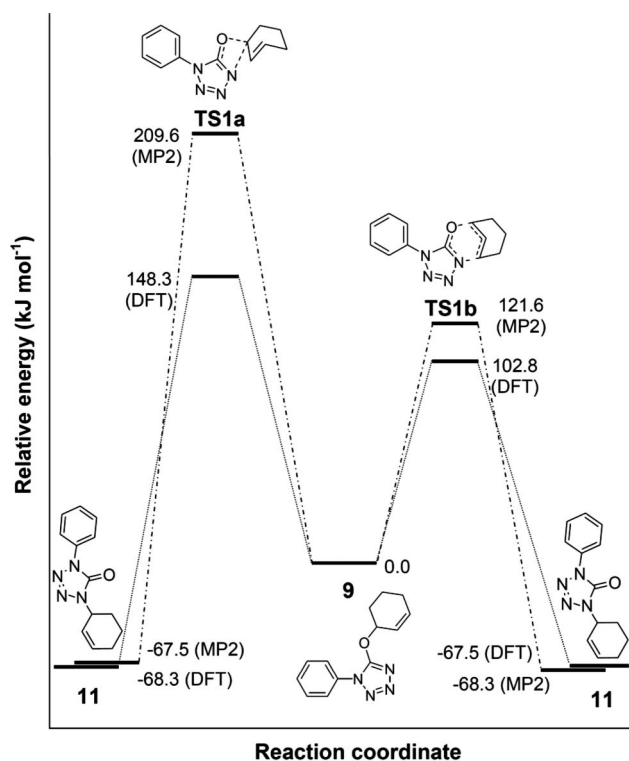


Fig. 2 Relative energies of the most stable stationary points for the thermal isomerization of 5-(cyclohex-2-enyloxy)-1-phenyl-1*H*-tetrazole (9) into 1-(cyclohex-2-enyl)-4-phenyl-1*H*-tetrazol-5(4*H*)-one (11) calculated at the DFT(B3LYP)/6-31G(d,p) (ΔE_G) and MP2/6-31G(d,p) (ΔE_d) levels.

of isomerization of 10 exhibits a prominent signal at δ 5.97–6.04 (Table 1 and Fig. 1S, ESI[†]), corresponding to the two vinyl protons, in agreement with the predicted spectra for compound 12, resulting from a [3,3]-shift mechanism, and no other signals that could correspond to compound 17 were detected, thus establishing compound 12 as the sole product of isomerization. (¹H-NMR spectra, ESI[†]).

Concerning the isomerization of ether 14, predicted ¹H-NMR spectra of the putative rearranged products reveal characteristic signals for the [1,3]- and [3,3]-migration products, compounds 18 and 15, respectively (Fig. 4). In particular, signals at δ 3.83 (CH₂) and 5.33 (CH) are expected for the product of [1,3]-migration, (18) and at δ 5.22–5.19 (CH₂) and 5.83 (CH) for the product of [3,3]-migration (15) (Table 2 and Fig. 4S, ESI[†]). The experimental ¹H-NMR spectrum of the product of isomerization of 14 shows prominent and well resolved signals corresponding to two doublets between δ 5.16–5.25 (CH₂), resulting from resonances of the two vinyl protons at one extreme of the double bond (*cis* and *trans*). These protons are coupled with the vinyl proton at the other extreme of the double bond, which corresponds to a doublet of doublets at 6.23–6.30 (CH) (Table 2 and Fig. 3S, ESI[†]). This pattern is clearly in agreement with the predicted spectra for compound 15, resulting from a [3,3]-shift mechanism, and no other signals that could correspond to compound 18 were detected. Thus, compound 15 appears to be the sole product of isomerization (¹H-NMR spectra, ESI[†]).

In conclusion, analysis of the ¹H-NMR spectra of the compounds obtained shows that tetrazolones 12 and 15 are the

Table 1 Experimental $^1\text{H-NMR}$ chemical shifts δ (ppm) of protons of the allylic system corresponding to the rearranged product of ether **10** (tetrazolone **12**), and predicted signals for putative [1,3]- and [3,3]-migration products (tetrazolones **17** and **12**)^{a,b}

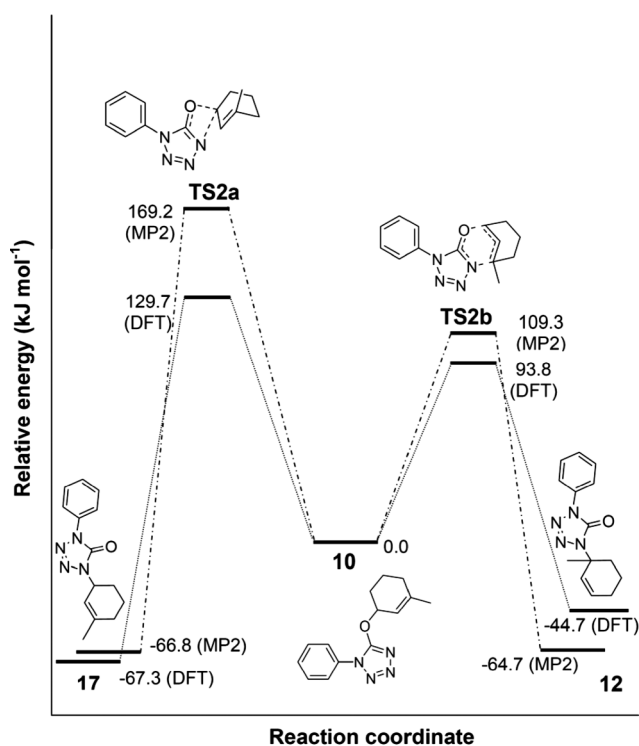
Atom Number		Experimental δ (ppm) (multiplicity; integration)	Predicted δ (ppm) for [1,3'] (multiplicity; integration) (17)	Predicted δ (ppm) for [3,3'] (multiplicity; integration) (12)
H4	CH	5.97–6.04 (m,2) ^c	4.06 (m,1)	5.59 (m,2) ^c
H9	CH	5.97–6.04 (m,2) ^c	5.37 (d,1)	5.59 (m,2) ^c

^a Experimental data ($^1\text{H-NMR}$ spectrum) is included as supplementary material. ^b Predicted $^1\text{H-NMR}$ shifts were acquired using the ChemDraw software. ^c Integration with value 2 due to overlapping of signals for H4 and H9, as predicted for the [3,3]-migration products.

Table 2 Experimental $^1\text{H-NMR}$ chemical shifts δ (ppm) of vinyl protons for the rearranged product of ether **14** (tetrazolone **15**) and predicted signals for putative products resulting from [1,3]- and [3,3]-migration (compounds **18** and **15**)^{a,b}

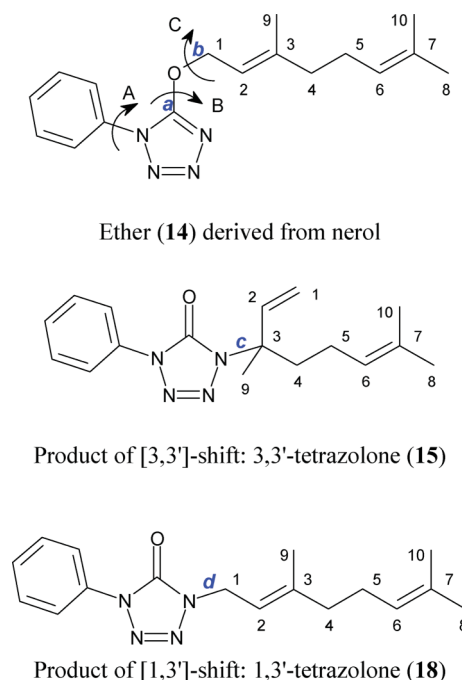
Atom Number		Experimental δ (ppm) (multiplicity; integration)	Predicted δ (ppm) for [1,3'] (multiplicity; integration) (18)	Predicted δ (ppm) for [3,3'] (multiplicity; integration) (15)
H4	CH_2	5.16–5.25 (m,2)	3.83 (d,2)	5.22/5.19 (m,2)
H5	CH	6.23–6.30 (m,1)	5.33 (t,1)	5.83 (m,1)

^a Experimental data ($^1\text{H-NMR}$ spectra) is included as supplementary material. ^b Predicted $^1\text{H-NMR}$ shifts acquired with ChemDraw software.

**Fig. 3** Relative energies of the most stable stationary points for the thermal isomerization of 5-(3-methylcyclohex-2-enyloxy)-1-phenyl-1*H*-tetrazole (**10**) into 1-(cyclohex-2-enyl)-1-methyl-4-phenyltetrazol-5-one (**12**) and 1-(3-Methylcyclohex-2-enyl)-4-phenyltetrazol-5-one (**17**) calculated at the DFT(B3LYP)/6-31G(d,p) (ΔE_c) and MP2/6-31G(d,p) (ΔE_{cl}) levels.

sole products of thermal rearrangement and arise from [3,3']-isomerization of ethers **10** and **14**, respectively.

In order to gather further information on the observed selectivity, the isomerizations were simulated theoretically by means of extensive DFT(B3LYP)/6-31G(d,p) and MP2/6-31G(d,p) calculations performed on *O*-allyl and *N*-allyl isomers and on putative transition state structures. Two possibilities were explored: [1,3']-

**Fig. 4** **Top:** Structure of allyl tetrazolyl ether derived from the allylic alcohol nerol: (*E*)-5-(3,7-dimethylocta-2,6-dienyloxy)-1-phenyl-1*H*-tetrazole (**14**). **Middle:** Structure of the rearrangement product resulting from [3,3']-sigmatropic migration of the allylic system: 1-(3,7-dimethylocta-1,6-dien-3-yl)-4-phenyl-1*H*-tetrazol-5(4*H*)-one (**15**). **Bottom:** Structure of the rearrangement product resulting from [1,3']-sigmatropic migration of the allylic system: (*E*)-1-(3,7-dimethylocta-2,6-dienyl)-4-phenyl-1*H*-tetrazol-5(4*H*)-one (**18**). Arrows, accompanied with letters A, B, C, show intramolecular conformational degrees of freedom similar to the ethers derived from the carbocyclic allylic alcohols **9** and **10**. Carbon atoms of the side chain are numbered, so that in all three systems (**14**, **15**, **18**) the same carbon atom retains the same number.

and [3,3']-sigmatropic migrations of the allylic system. The results obtained are presented and discussed below, and clearly confirm

Table 3 Conformationally relevant geometric parameters and relative energies of conformers of 5-(3-methylcyclohex-2-enyloxy)-1-phenyl-1*H*-tetrazole **10** [in brief: Ether **10** (*R*)] and corresponding isomeric 1-(3-methylcyclohex-2-enyl)-4-phenyltetrazol-5-one **17** [in brief: Tetrazolone **17** (*R*)] and isomeric 1-(cyclohex-2-enyl)-1-methyl-4-phenyltetrazol-5-one **12** [in brief: Tetrazolone **12** (*S*)] calculated at the DFT(B3LYP)/6-31G(d,p) level of theory

Compound / Conformer		Dihedral angle/°				Relative energy/kJ mol ⁻¹		
No.	Ether 10 (<i>R</i>)	A	B	C	D	ΔE_{el}	ΔE_{ZPE}	ΔE_G
1	Ph ⁺ TTG ⁻	28.3	176.7	-158.1	-58.8	0.00	0.00	0.00
2	Ph ⁺ TG ⁻ G ⁻	23.7	178.3	-83.0	-59.6	-0.28	0.06	0.82
3	Ph ⁻ TTG ⁻	-27.6	-175.6	-162.3	-59.3	0.13	0.12	0.03
4	Ph ⁻ TG ⁻ G ⁻	-19.1	-175.6	-82.0	-59.1	0.15	0.28	0.51
5	Ph ⁻ TG ⁻ G ⁺	-23.8	-176.6	-80.8	60.6	1.12	1.23	2.14
6	Ph ⁺ TG ⁻ G ⁺	22.0	178.5	-81.1	60.6	1.74	1.67	0.20
7	Ph ⁺ TTG ⁺	27.0	177.2	-155.2	60.6	2.30	2.45	3.15
8	Ph ⁻ TTG ⁺	-26.4	-178.2	-158.2	60.8	2.83	2.96	3.56
9	Ph ⁺ TG ⁺ G ⁺	28.7	170.1	68.7	60.8	11.31	11.45	13.17
10	Ph ⁻ TG ⁺ G ⁺	-28.1	177.9	65.9	60.8	11.97	11.86	12.46
11	Ph ⁺ TG ⁺ G ⁻	29.3	159.4	79.9	-53.1	16.08	15.91	16.33
12	Ph ⁻ TG ⁺ G ⁻	-28.5	172.2	73.8	-52.4	17.21	17.01	17.26
No.	Tetrazolone 17 (<i>R</i>)	A	C	D	ΔE_{el}	ΔE_{ZPE}	ΔE_G	
1	CG ⁺	-0.5	3.1	60.6	-68.58	-67.16	-66.80	
2	CG ⁻	0.0	10.6	-59.0	-67.67	-66.03	-65.93	
3	TG ⁺	3.8	179.1	60.9	-65.06	-63.62	-62.47	
4	TG ⁻	0.1	-170.2	-57.4	-62.56	-60.75	-59.03	
No.	Tetrazolone 12 (<i>S</i>)	A	C	D	ΔE_{el}	ΔE_{ZPE}	ΔE_G	
1	G ⁺ G ⁺	-0.5	61.4	61.0	-49.46	-48.16	-44.67	
2	TG ⁺	-1.8	-177.9	59.0	-48.57	-47.21	-43.67	
3	TG ⁻	2.3	-176.5	-61.5	-46.13	-44.70	-41.46	
4	G ⁺ G ⁻	1.0	61.7	-60.1	-45.90	-44.64	-41.61	
5	G ⁻ G ⁻	-1.7	-59.9	-59.9	-45.06	-43.85	-40.40	
6	G ⁻ G ⁺	-0.7	-78.6	58.5	-41.10	-40.31	-38.59	
No.	TS type	Distance/pm				ΔE_{el}	ΔE_{ZPE}	ΔE_G
1	1,3'-shift	OC(1)	OC(3)	NC(1)	NC(3)	144.65	133.22	131.05
2	1,3'-shift	276.3	339.0	275.0	399.1	143.44	131.97	129.76
3	3,3'-shift	271.4	404.9	270.1	335.1	106.21	98.12	103.00
4	3,3'-shift	245.9	343.3	338.9	242.7	98.93	90.58	93.75
		239.8	341.2	335.0	240.9			

Definition of the geometric parameters (see also Fig. 1 for the graphical representation). Compound "Ether **10**" (*R*-enantiomer): A is defined as CCNC dihedral angle; B is defined as *N*-COC dihedral angle; C is defined as COC(1)C(6); D is defined as C(1)C(6)C(5)C(4). Compound "Tetrazolone **17**" resulting from 1,3'-shift (*R*-enantiomer): A is defined as CCNC dihedral angle; dihedral angle "B" (analogous of ether) is not applicable; C is defined as C-NC(1)H dihedral angle; D is defined as C(1)C(6)C(5)C(4) dihedral angle. Compound "Tetrazolone **12**" resulting from 3,3'-shift (*S*-enantiomer): A is defined as CCNC dihedral angle; dihedral angle "B" (analogous of ether) is not applicable; C is defined as C-NC(1)C(6) dihedral angle; D is defined as C(1)C(6)C(5)C(4) dihedral angle. "TS" stands for transition state. Numbering of the carbon atoms corresponds to that of the starting compound. Nitrogen atom is N(5) of the ether. All relative energies are calculated with respect to Ph⁺TTG⁻ conformer (No. 1) of Ether **10**. ΔE_{el} , ΔE_{ZPE} , ΔE_G state for the relative electronic, zero-point-corrected and Gibbs free energy (at 298.15 K), respectively. The absolute values calculated for Ph⁺TTG⁻ at the DFT(B3LYP)/6-31G(d,p) level are: $E_{el} = -837.319052$; $E_{ZPE} = -837.031930$, $E_G = -837.077882$ hartree.

that the [3,3']-shift is kinetically favoured over the [1,3']-shift for the three allylic ethers of tetrazole investigated.

2.2. Isomerization of 5-(cyclohex-2-enyloxy)-1-phenyl-1*H*-tetrazole (**9**) and 5-(3-methylcyclohex-2-enyloxy)-1-phenyl-1*H*-tetrazole (**10**)

2.2.1. Molecular geometry. Fig. 1 shows the structure of allyl tetrazolyl ethers derived from the carbocyclic allylic alcohols cyclohex-2-enol (**7**, X = H) and 3-methylcyclohex-2-enol (**8**, X = CH₃). The starting compounds (ethers **9** and **10**) have four intramolecular rotational degrees of freedom (designated in Fig. 1 by arrows) that may result in different conformers. These include: (i) relative orientation of the phenyl and tetrazolyl rings (dihedral angle A); (ii) relative orientation of the allylic ether substituent

and the phenyl ring (dihedral angle B). For this dihedral, only the starting *trans* orientation was considered since only in this case the allylic fragment is aligned properly for intramolecular migration; (iii) relative orientation of the cyclohex-2-enol and tetrazole rings (dihedral angle C). It is important to note that the carbon atom C(1) is chiral. In the present study all calculations were carried out for the *R*-enantiomer of the starting compound; (iv) conformation of the cyclohex-2-enol ring (dihedral angle D).

The calculated energetic and geometric parameters of the equilibrium structures are collected in Tables 1S (DFT) and 2S (MP2), ESI,[†] for compounds **9** and **16** (X = H) and in Tables 3 (DFT) and 4 (MP2) for compounds **10** and **17** (X = CH₃). As mentioned in the introduction, allyl tetrazolyl ethers may undergo thermal isomerization to the corresponding tetrazolones. Such isomerizations were simulated theoretically in the present

Table 4 Conformationally relevant geometric parameters and relative energies of conformers of 5-(3-methylcyclohex-2-enyloxy)-1-phenyl-1*H*-tetrazole **10** [in brief: Ether **10** (*R*)] and corresponding isomeric 1-(3-methylcyclohex-2-enyl)-4-phenyltetrazol-5-one **17** [in brief: Tetrazolone **17** (*R*)] and isomeric 1-(cyclohex-2-enyl)-1-methyl-4-phenyltetrazol-5-one **12** [in brief: Tetrazolone **12** (*S*)] calculated at the MP2/6-31G(d,p) level of theory

Compound / Conformer		Dihedral angle/°				Relative Energy/kJ mol ⁻¹
No.	Ether 10 (<i>R</i>)	A	B	C	D	ΔE_{el}
1	Ph ⁺ TTG ⁻	-34.9	-172.8	-168.9	-62.2	0.00
2	Ph ⁺ TTG ⁻	36.4	-179.2	-165.3	-61.8	0.03
3	Ph ⁺ TG ⁻ G ⁻	33.3	174.9	-78.9	-62.4	1.15
4	Ph ⁻ TG ⁻ G ⁻	-33.8	-176.8	-79.8	-62.2	1.58
5	Ph ⁻ TG ⁻ G ⁺	-34.4	-176.7	-78.1	63.3	4.69
6	Ph ⁺ TTG ⁺	35.4	177.9	-161.5	63.5	4.85
7	Ph ⁺ TG ⁺ G ⁺	34.6	176.2	-76.8	63.3	5.07
8	Ph ⁻ TTG ⁺	-34.9	-177.4	-163.2	63.5	5.16
9	Ph ⁺ A ⁺ G ⁻ G ⁻	38.6	89.7	105.8	-59.6	10.57
10	Ph ⁺ TG ⁺ G ⁺	36.6	165.6	72.0	62.8	10.61
11	Ph ⁻ TG ⁺ G ⁺	-37.0	175.8	68.4	62.9	11.40
12	Ph ⁻ A ⁺ G ⁺ G ⁻	-40.4	131.4	102.7	-57.9	16.99
No.	Tetrazolone 17 (<i>R</i>)	A	C	D	ΔE_{el}	
1	Ph ⁺ CG ⁻	22.0	27.2	-62.3	-67.29	
2	Ph ⁻ CG ⁻	-22.1	28.2	-62.4	-67.28	
3	Ph ⁺ CG ⁺	22.7	9.1	63.3	-64.92	
4	Ph ⁻ CG ⁺	-23.0	10.0	63.3	-64.92	
5	Ph ⁺ TG ⁺	23.6	179.9	63.4	-63.11	
6	Ph ⁻ TG ⁺	-23.4	-179.8	63.4	-62.99	
7	Ph ⁺ TG ⁻	25.5	-163.1	-60.3	-62.58	
8	Ph ⁻ TG ⁻	-25.4	-162.8	-60.3	-62.41	
No.	Tetrazolone 12 (<i>S</i>)	A	C	D	ΔE_{el}	
1	Ph ⁺ G ⁺ G ⁺	24.5	61.5	64.4	-64.73	
2	Ph ⁻ G ⁺ G ⁺	-24.1	61.8	64.4	-64.68	
3	Ph ⁺ TG ⁺	24.6	-175.2	62.5	-63.43	
4	Ph ⁻ TG ⁺	-23.7	-175.3	62.5	-63.28	
5	Ph ⁻ TG ⁻	-24.4	-176.9	-64.1	-58.90	
6	Ph ⁺ TG ⁻	24.8	-177.0	-64.1	-58.88	
7	Ph ⁺ G ⁺ G ⁻	24.6	60.5	-62.5	-58.56	
8	Ph ⁻ G ⁺ G ⁻	-23.9	60.7	-62.5	-58.52	
9	Ph ⁻ G ⁻ G ⁻	-24.0	-60.8	-62.4	-57.78	
10	Ph ⁺ G ⁻ G ⁻	23.9	-61.0	-62.3	-57.62	
11	Ph ⁻ G ⁻ G ⁺	-26.5	-84.5	62.3	-56.22	
12	Ph ⁺ G ⁻ G ⁺	25.3	-85.1	62.4	-56.05	
		Distance/pm				
No.	TS type	OC(1)	OC(3)	NC(1)	NC(3)	ΔE_{el}
1	1,3'-shift	266.7	284.7	285.9	368.8	188.21
2	1,3'-shift	267.0	416.6	316.6	303.1	169.24
3	3,3'-shift	210.6	317.8	321.0	218.2	117.96
4	3,3'-shift	220.9	324.7	327.2	223.5	109.31

For the definition of the geometric parameters see caption of Table 3 and also Fig. 1 for the graphical representation. All relative electronic energies (ΔE_{el} , in kJ mol⁻¹) are calculated with respect to Ph⁻TTG⁻ conformer (No. 1) of Ether **10**. The absolute value calculated for Ph⁻TTG⁻ conformer at the MP2/6-31G(d,p) level is $E_{el} = -834.810723$ hartree.

study. Two possibilities were explored: [1,3']- and [3,3']-sigmatropic migrations of the allylic system. The products resulting from such migrations (tetrazolones **11**, **12**, **16** and **17**) are shown in Fig. 1 (along with ethers) and their parameters are included in Tables 3, 4, 1S and 2S, ESI,† also. In the course of theoretical studies, it was found that the [1,3']-sigmatropic shift does not change the stereochemistry of the chiral carbon atom C(1). However, during the [3,3']-sigmatropic shift, the stereochemistry around the C(1) carbon atom of the tetrazolone product changes from *R* to *S*. The X group (X = H or X = CH₃) remains the lowest-priority substituent around the C(1) atom in the course of the [3,3']-shift, while the heteroatom (O in ether; N in tetrazolone) remains the highest priority substituent. The change of chirality is related

to the switch of positions of the second (-CH=C) and third (-CH₂-C) priority groups around C(1). The additional difference between the [1,3']- and [3,3']-shift is the nature of the lowest-priority substituent around the C(1) atom. In the case of [1,3']-shift, it is always H. In the case of [3,3']-shift, it is the X functional group. If X = H, the molecule resulting from the [3,3']-sigmatropic shift is the mirror image of the molecule produced in the [1,3']-sigmatropic shift. If X = CH₃, the two sigmatropic shifts, [1,3'] and [3,3'], produce two distinct isomers.

Due to the difference in chirality, the two tetrazolones resulting from [1,3']- and [3,3']-sigmatropic shift are named, for brevity, in Tables 3, 4, 1S and 2S, ESI,† as tetrazolone (*R*) and tetrazolone (*S*), respectively. However, it should be noted here that this difference

in chirality is not the only difference between them. The most important difference is the change in the position of the substituent X relatively to the tetrazolone ring.

Comparative analysis of Tables 3, 4, 1S and 2S, ESI,† shows some interesting trends. First of them is the relative orientation of the phenyl ring with respect to the ring to which it is attached (tetrazole (ether) or tetrazolone), *i.e.* values of dihedral angle A. The exchange of the substituent X (H or CH₃) does not have influence on this parameter. However, the theory levels and the nature of the tetrazolic ring do have influence. In the ether, the phenyl ring is not co-planar with the tetrazole ring. The calculated inter-ring angles lie in a narrow interval equal to $26 \pm 4^\circ$ (DFT) or $36 \pm 3^\circ$ (MP2). In tetrazolones, calculations at the DFT level predict the two rings to be essentially co-planar, while the MP2 calculations show a well-defined deviation from co-planarity: $24 \pm 2^\circ$. In the latter case, the inter-ring angle is definitely not *cis*, since it has two non-equivalent orientations, but still this dihedral is not large enough to be designated as *gauche*. Therefore, we adopted, in the names of conformers in Tables 3, 4, 1S and 2S, ESI,† a non-traditional designation Ph⁺ or Ph⁻, which unequivocally describes the orientation of the dihedral angle A. Variations from Ph⁺ to Ph⁻ (if the dihedral angle A is different from *cis*), produce pairs of conformers of approximately equal energy, *i.e.* the conformational preference is defined by other conformational degrees of freedom. It is important to note here that the MP2 calculated values of dihedral angle A always show a higher degree of non-co-planarity comparing to the calculations of the same structures at the DFT level. This is due to the fact that MP2 calculations better describe the non-covalent interactions (between the tetrazole and phenyl rings) existing in the studied molecules.

Dihedral angle B occurs only in the two ether (starting) compounds (9 and 10). As it was mentioned, the initial value of this dihedral angle selected for optimizations was chosen around the *trans* orientation, which permits the occurrence of the sigmatropic shifts. Upon optimizations, most of conformers retained the *trans* orientation for the dihedral angle B and stayed around $179 \pm 5^\circ$ (DFT) or $180 \pm 5^\circ$ (MP2). A few exceptions will be discussed below.

A very regular pattern of values was also found for dihedral angle D, describing the conformation of the partially saturated cyclohex-2-enol ring. With two possible directions of the internal rotation, dihedral angle D assumed in all conformers only two values, G⁺ and G⁻. For both ether derivatives and for the tetrazolones, the calculated absolute values of the dihedral angle D were found to fall in a very narrow range and amount to $60 \pm 1^\circ$ (DFT) and $63 \pm 1^\circ$ (MP2). A very high reproducibility of the numeric values of the dihedral angle D indicates the rigidity of the cyclohex-2-enol ring. In a few conformers, larger deviations from these values were found. These cases will be commented on below as well.

Dihedral angle C is the most flexible conformational degree of freedom. In the ether compounds, three groups of minima per 360° rotation of the cyclohex-2-enol fragment around the O–C(1) bond were found. In the ethers of *R*-chirality, the corresponding optimized values of the COC(1)C(6) dihedral angle densely group around the *trans* ($-159 \pm 4^\circ$, DFT and $-165 \pm 4^\circ$, MP2) and G⁻ ($-82 \pm 2^\circ$, DFT and $-78 \pm 2^\circ$, MP2) conformations, while they are loosely scattered around the G⁺ orientation ($72 \pm 8^\circ$, DFT and $87 \pm 20^\circ$, MP2). Note that G⁺ conformers consistently have much

higher relative energies, exceeding the T and G⁻ conformers by more than 10 (DFT) or 5 (MP2) kJ mol⁻¹.

Upon the [1,3]-sigmatropic shift, the dihedral angle C in the tetrazolone product corresponds to the rotation around the newly formed N–C(1) bond. Unlike for the case of the ether, only two minima were found per 360° rotation in the tetrazolone, being grouped around the *cis* and *trans* orientation of the CNCH dihedral angle. All the *cis* conformers around the dihedral angle C are systematically more stable than the *trans* conformers in these products. For the methylated compound 12, resulting from the [3,3]-sigmatropic shift, substitution of H by CH₃ at C(1) changes remarkably the energy profile for the rotation around N–C(1) bond: for one 360° turn, compound 11 has only two minima, while the methylated compound 12 exhibits three minima. For the tetrazolone of *S*-chirality, the corresponding optimized values (both DFT and MP2) of the COC(1)C(6) dihedral angle form two dense groups, *trans* (from -175° to -178°) and G⁺ (from 60° to 62°), as well as one loose group around G⁻ orientation (from -60° to -85°).

Now that all the conformationally important degrees of freedom have been briefly introduced, it is important to comment on the consistent patterns and on the exceptions. In the starting compounds 9 and 10, at all levels of theory, there is a group of four conformers that have relative energies of 10 or more kJ mol⁻¹, compared to the most stable form. All these conformers have one common geometric parameter: the dihedral angle C [or more precisely, COC(1)C(6)] adopts a G⁺ orientation. This is equivalent to saying that the dihedral angle COC(1)C(2) should adopt a *cis* orientation. Such an orientation results in a crowded geometry which brings the cyclohex-2-enol and tetrazole rings into a very close vicinity. These crowded geometries become even more strained when the cyclohex-2-enol units assume a G⁻ conformation. In order to compensate for such unfavourable orientation, the internal twist of the cyclohex-2-enol ring (dihedral angle D) reduces to about -53° (while the strain-free value is *ca.* -59°). At the DFT level of theory, such geometric changes of the Ph(±)TG⁺G⁻ conformers (No. 11 and 12, Tables 3 and 1S, ESI†) are accompanied by an additional destabilization of 5 kJ mol⁻¹ compared to the Ph(±)TG⁺G⁺ conformers (No. 9 and 10). Additionally, dihedral angle B (normally “*trans*”) strongly deviates from the geometry characteristic of the unstrained conformers, reaching in the crowded conformers distorted values down to 160° (see Tables 3 and 1S, ESI†).

The MP2 calculations “deal with the situation” in a slightly different way. Instead of the distortion of the dihedral angle D (*i.e.* forcing twist of the rigid cyclohex-2-enol ring), a stronger deviation of dihedral angle B from the *trans* orientation has occurred during the optimization of geometries. Such deviation reached the dihedral angles B as low as 90° (see Tables 4 and 2S, ESI†, conformers Ph⁺A⁺G⁺G⁻, “A” stands for “*ant*iclinal”). This geometry change not only avoids the crowded orientation of the two rings, but also apparently creates a stabilizing interaction between them. Such stabilization is even capable of compensating partially for the distortion of the dihedral angle B: the relative energy of the corresponding conformers decreases from 16.3 kJ mol⁻¹ (DFT level, Ph⁺TG⁺G⁻ form, No. 11, Table 3) to 10.6 kJ mol⁻¹ (MP2 level, Ph⁺A⁺G⁺G⁻ form, No. 9, Table 4).

Now let us discuss the calculated energies in more detail. Unfortunately, the vibrational characterization of the entire set

of the optimized structures at the MP2 level is beyond practical limitations. For a few selected optimized structures, the vibrational MP2 calculations were carried out numerically. This was extremely time-consuming but confirmed the expected nature of the optimized stationary points. Under these circumstances, the DFT vibrational calculations (Tables 3 and 1S, ESI†) provide some useful information. Comparison of ΔE_{el} with ΔE_{ZPE} and with ΔE_{G} shows that accounting for the zero-point vibrational energy, as well as accounting for the thermochemistry at room temperature does not significantly change the position of conformers on the relative energy scale: the most stable forms remain most stable, the order of stability is mostly preserved, the differences in relative energies do not exceed a few kJ mol^{-1} upon moving from ΔE_{el} to ΔE_{ZPE} and to ΔE_{G} . This is true for all studied compounds. We extrapolated this trend to the MP2 calculations, assuming that the order of the calculated electronic energies should describe, fairly enough, the stabilities of the studied compounds under standard conditions (at 298.15 K).

2.2.2. Mechanism of isomerization. In all calculations, the relative zero level of energy was chosen to be the energy of the most stable ether conformer. The calculated relative energies for the sigmatropic shifts are shown in the last section of each of the Tables (3, 4, 1S and 2S, ESI†) and in Fig. 2 and 3 (energy profiles for isomerizations) for derivatives **9** and **10**. The structures of transition states are most important in this study, as they dictate the barriers to the two different isomerization pathways. The optimized Cartesian coordinates of all the transition states found in this study are collected in the ESI,† along with their calculated electronic energies and net dipole moments. It should be noted as well that, for each of the studied isomerizations, two alternative parallel pathways were found.‡ The energies and dipole moments of these parallel transition states are qualitatively similar.

The calculations show that the $[1,3']$ -sigmatropic shifts are energetically more demanding as compared with the $[3,3']$ -shifts. At the DFT level of theory, the transition states for the $[1,3']$ -shifts are above 148 kJ mol^{-1} ($X = \text{H}$, **TS1a**) or 130 kJ mol^{-1} ($X = \text{CH}_3$, **TS2a**), while at the MP2 level these values increase up to at least 209 and 169 kJ mol^{-1} respectively. The calculated barriers for the $[3,3']$ -shifts were found to be much lower: 103 and 94 kJ mol^{-1} (DFT); 121 and 109 kJ mol^{-1} (MP2) (see **TS1b** and **TS2b** in Fig. 2 and 3). This means that kinetically the $[3,3']$ -shifts should dominate over the $[1,3']$ -shifts. According to all calculations, tetrazolones formed in the processes of sigmatropic shifts are far more stable than the starting ethers. For the $[1,3']$ -shifts, in ethers **9** and **10**, the gain in stability constitutes about $67\text{--}68 \text{ kJ mol}^{-1}$ (for the most stable tetrazolone conformer), both at the DFT and MP2 levels. For the $[3,3']$ -shifts and $X = \text{H}$, the final tetrazolone product (**11**) is identical with that of the $[1,3']$ -shifts, so the process of isomerization should occur *via* the $[3,3']$ -shift, since it requires much lower activation energy (see Fig. 2). For the methylated compound (**10**, $X = \text{CH}_3$), the structure of the tetrazolone formed (**12** or **17**) is unique to the mechanism. The DFT calculations (see Table 3) predict the product of the $[3,3']$ -shift (tetrazolone **12** “S”) to be higher in energy by as much as 22 kJ mol^{-1} as compared to the product of the $[1,3']$ -shift (tetrazolone

17 “R”). However, the MP2 calculations carried out for the same compounds (see Table 4), show only a marginal difference (*ca.* 2.6 kJ mol^{-1}) between the two products, *i.e.* they can be considered essentially isoenergetic (Fig. 3). Therefore, the control over the outcome of the isomerization reaction should be kinetic and the expected product should be that corresponding to the $[3,3']$ -shift, compound **12**. As discussed above, the experimental data are in agreement with this conclusion, showing that the tetrazolone adopts the structure consistent with the $[3,3']$ -shift mechanism ($^1\text{H-NMR}$ spectra, ESI†).

2.3. Isomerization of (*E*)-5-(3,7-dimethylocta-2,6-dienyloxy)-1-phenyl-1*H*-tetrazole (**14**)

2.3.1. Molecular geometry. Fig. 4 shows the structure of tetrazolyl ether (**14**) derived from the allylic alcohol nerol. Ether **14** is not chiral and has eight intramolecular rotational degrees of freedom. Three of them (A, B, C, designated in Fig. 4 by arrows) are similar to ethers **9** and **10**. The remaining five dihedral angles correspond to the internal rotations of the carbon atom side-chain (around the $\text{C}(1)\text{--}\text{C}(2)$, $\text{C}(2)=\text{C}(3)$, $\text{C}(3)\text{--}\text{C}(4)$, $\text{C}(4)\text{--}\text{C}(5)$, $\text{C}(5)\text{--}\text{C}(6)$ bonds). The products of the intramolecular shifts, tetrazolones **15** and **18**, are also shown in Fig. 4. In product **15** of the $[3,3']$ -shift, carbon atom $\text{C}(3)$ becomes chiral, while no chirality is acquired in product **18** of the $[1,3']$ -shift. The resulting tetrazolones have six (**15**) and seven (**18**) conformational degrees of freedom.

The large flexibility of species **14**, **15** and **18** may result in over a hundred possible conformers which makes the complete characterization of their conformational space impractical. Despite the large number of intramolecular degrees of freedom, several trends were revealed in the course of optimizations. These trends helped to localize the set of most stable conformers. The calculated energetic and geometric parameters for the most relevant equilibrium structures of ether (*E*)-5-(3,7-dimethylocta-2,6-dienyloxy)-1-phenyl-1*H*-tetrazole (**14**) and of its isomerization products, tetrazolones **15** [1-(3,7-dimethylocta-1,6-dien-3-yl)-4-phenyl-1*H*-tetrazol-5(4*H*)-one] and **18** [(*E*)-1-(3,7-dimethylocta-2,6-dienyl)-4-phenyl-1*H*-tetrazol-5(4*H*)-one], are collected in Tables 3S (DFT) and 4S (MP2), ESI.†

For dihedral angle A, describing the relative orientation of the phenyl and tetrazole rings, the trends for compounds **14**, **15**, **18** were found to be the same as for **9**, **10**, **11**, **12**, **16** and **17**. The absolute value of the inter-ring angle in ether **14** amounts to *ca.* $25 \pm 2^\circ$ (DFT) or $34 \pm 2^\circ$ (MP2). In tetrazolones **15** and **18**, the DFT method predicts the two rings to be co-planar, while the MP2 calculations result in the twist of $23 \pm 2^\circ$. For dihedral angle B, as in the case of ethers **9** and **10**, out of the two possibilities (*cis* and *trans*), only the starting *trans* orientation was considered in ether **14**. Only in this case is the allylic fragment aligned properly for intramolecular migration.

For the allylic fragments, the atoms directly linked to the carbons forming the $\text{C}=\text{C}$ double bonds are located approximately in one plane. There are two such groups in compounds **14** and **18**: one group is composed by carbon atoms 1, 2, 3, 4, 9 and the other group consists of atoms 5, 6, 7, 8, 10 (Fig. 4). Moreover, in the most stable conformers found, the planes formed by these two groups of atoms tend to be parallel to each other. The orientation of the bonds $\text{O--C}(1)$ (**14**) or $\text{N--C}(1)$ (**18**) and $\text{C}(4)\text{--}\text{C}(5)$ (**14** and **18**) is

‡The conformational flexibility of the migrating fragment in the nerol derivative may increase this number.

not parallel to the above-mentioned “five-atom-planes” and the intramolecular rotations around these bonds represent the main conformational variable.

At the DFT level (Table 3S, ESI†), ether **14** adopts many conformational structures that are very close in energy to each other: at least 18 structures fall into a 0–5 kJ mol⁻¹ energy interval. It is interesting to note that correction for the calculated Gibbs free energies (at 298.15 K) retains these 18 structures in the same energy gap. However, the order of their relative energy changes: it is sensitive to the presence of a large number of the low-frequency vibrational modes that contribute most to the thermal corrections. Regarding the equilibrium geometries of these 18 structures, the nerol residue assumes an extended conformation with the two 5-atom mini-planes being essentially co-planar. The entire nerol residue then adopts a multitude of different orientations with respect to the tetrazole ring, depending on the values of dihedral angle C, which assumes all of the T, G⁺ and G⁻ positions.

The calculated DFT energies of the product of [3,3′]-shift, tetrazolone **15**, show a stabilization in energy by about 44 kJ mol⁻¹, with respect to ether **14**, comparing the two most stable respective conformers. For the product of [1,3′]-shift, tetrazolone **18**, the DFT-calculated stabilization is much more pronounced and amounts to about 79 kJ mol⁻¹. In all cases, the most stable conformations of **15** and **18** correspond to a distended configuration of the nerol residue, which is oriented approximately perpendicularly to (“away from”) the tetrazolone ring. The theoretical finding obtained on the basis of the DFT calculations (Table 3S, ESI†), should imply that the isomerization of ether **14**, if thermochemically controlled, should proceed *via* the [1,3′]-shift mechanism, which contradicts the experimental finding showing that the resulting product is formed *via* the [3,3′]-shift. The theoretical explanation of this discrepancy represented one of the main challenges of this study and could be successfully solved with recourse to *ab initio* calculations.

The *ab initio* calculations were carried out at the MP2/6-31G(d,p) level of theory. The geometry optimizations were started from the equilibrium geometries obtained previously at the DFT(B3LYP)/6-31G(d,p) level. Adopting such an approach, optimization of a single structure at the MP2/6-31G(d,p) level took between 2 and 10 days of the processor time which is about one order of magnitude higher than was required to complete the DFT calculations. The MP2 calculations took several months overall. The conformationally relevant dihedral angles, for the MP2 optimized geometries, of compounds **14**, **18** and **15** are presented in Table 4S, ESI.† Anticipating the discussion of the equilibrium MP2 geometries, it should be stated here that the main result of the MP2 calculations is in agreement with the experimental observation: tetrazolone **15** resulting from the [3,3′]-shift was predicted energetically more stable than tetrazolone **18** resulting from the [1,3′]-shift!

The different order of the relative stabilities (with respect to ether **14**) of tetrazolones **15** and **18** at the MP2 and DFT levels of theory was achieved at the expense of the strikingly different equilibrium geometries obtained with these two methods. Fig. 5 compares the geometries of the most stable forms of the two tetrazolones. In the DFT calculations the nerol residue adopts a distended conformation, which is oriented approximately perpendicularly to the plane of the tetrazole moiety. In the MP2 calculations, the nerol residue tends to assume an orientation parallel to the tetrazole

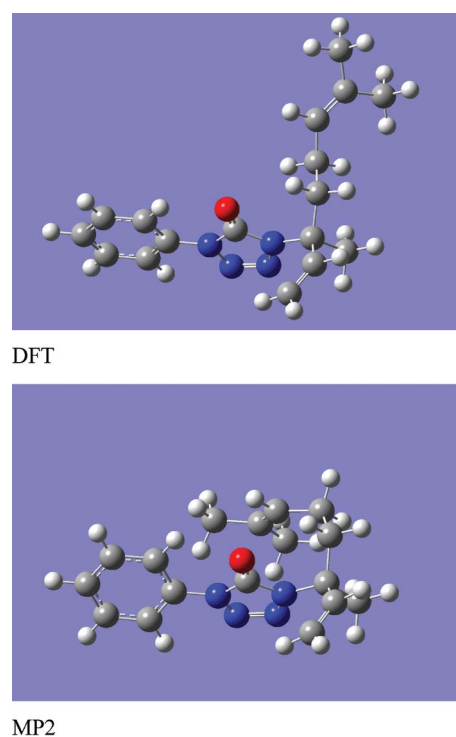


Fig. 5 Equilibrium geometries of the most stable structures of tetrazolone **15** (product of the [3,3′]-shift) resulting from the optimizations at the DFT and MP2 levels of theory. For reference, the orientation of the tetrazolone moiety in the figure was kept the same.

moiety, as much as the anchor *N* atom allows it. The latter (MP2) geometry suggests the importance of the π – π stacking interaction in tetrazolones derived from nerol.

It is known that the SCF based methods, like DFT(B3LYP) are unable to predict local minima on the potential energy surfaces for π – π stacked systems.²⁷ Only calculations at the MP2 theory level were successful in finding local minima for stacked dimers of quinine–pyrimidine,²⁸ uracil–thymine²⁹ and other *N*-heteroaromatic systems.³⁰ In such calculations, the stabilization energies of the stacking interaction ranged from 12 to 25 kJ mol⁻¹, while an equilibrium interplane distance of about 3.2 Å was found.³⁰

It is interesting to note that the most stable tetrazolone structure, found at the MP2 level in this study, corresponds to product **15** of the [3,3′]-isomerization (tetrazolone **15**, conformer 1, Table S4†). In this conformer, the interatomic distances between the carbon atom of the tetrazole ring C(T) and the two carbon atoms forming a double bond, C(6) and C(7), were found to be 2.99 and 3.49 Å, respectively. Such distances, as well as the pronounced stabilization of tetrazolone **15**, suggest existence of a π – π interaction in this structure. Indeed, the natural bond orbital (NBO) analysis reveals a strong overlap between the π -electron systems of tetrazole ring and the terminal C=C bond (see Fig. 6).

The most stable structures found at the MP2 level of theory for compounds **14**, **15** and **18** were used as the initial guess geometries for the recurrent optimizations at the DFT level. The most stable MP2 form of **15**, after re-optimization at the DFT level, distanced the side chain away from the tetrazole fragment. The C(T)–C(6) and C(T)–C(7) distances increased to 3.23 and 3.84 Å, respectively. The relative change of geometry after such

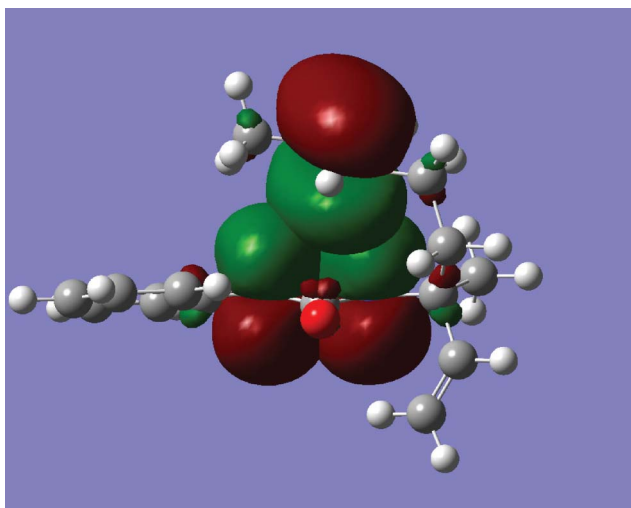
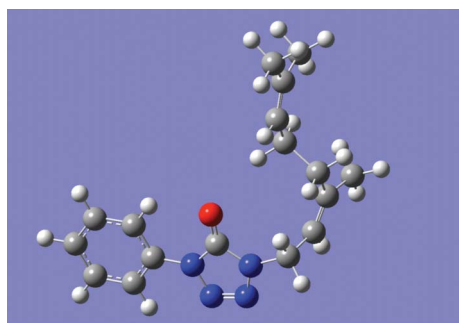


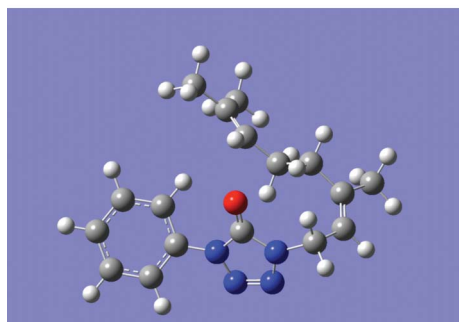
Fig. 6 Selected π -orbitals of the tetrazolone moiety and π -orbital of the terminal C=C bond of the nerol residue in the most stable conformer of tetrazolone **15**. Note co-planarity of the two π -electron systems and substantial orbital overlap.

re-optimization was not very significant: the $\text{TA}^+\text{TG}^+\text{A}^-$ orientation of the conformationally sensitive dihedral angles remained the same. However, in terms of the relative energy, the $\text{TA}^+\text{TG}^+\text{A}^-$ conformer moved from position 1 (MP2) up to position 5 (DFT). The most stable DFT conformer changed to $\text{TA}^+\text{T TA}^+$ which corresponds to the unfolded nerol residue (see Fig. 5).

Similar trends were also found for tetrazolone **18** (see Fig. 7): the most stable geometries correspond to the folded structures at



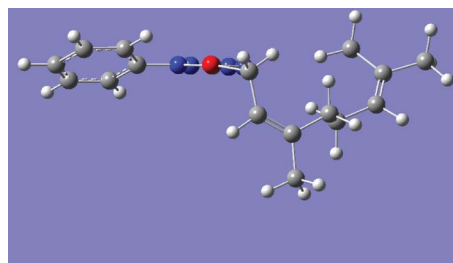
DFT



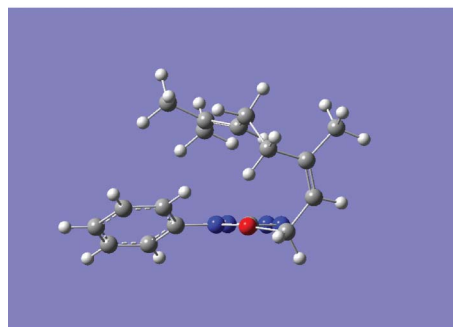
MP2

Fig. 7 Equilibrium geometries of the second most stable structures of tetrazolone **18** (product of the [1,3 γ]-shift) resulting from the optimizations at the DFT and MP2 levels of theory. For reference, the orientation of the tetrazolone moiety in the figure was kept the same.

the MP2 level, and to the distended structures at the DFT level of optimization. The same situation was also found for ether **14** where the two most stable respective geometries (DFT and MP2) do not have even a slight geometrical resemblance (see Fig. 8). An even more striking result was obtained when the most stable (in the MP2 energy scale) geometry of **14** was subjected to DFT optimization. The resulting structure, while a local minimum, turned to be the least stable among all DFT-optimized structures (Tables 3S and 4S, ESI †).



DFT



MP2

Fig. 8 Equilibrium geometries of the most stable structures of ether **14** resulting from optimizations at the DFT and MP2 levels of theory. For reference, the orientation of the tetrazolone moiety in figure was kept the same (viewed along the OC axis).

A question arises: “if the stabilization in tetrazolone **15** due to the non-bonded interactions is important, could a similar stabilization take place in **18**?” In order to answer this question it is interesting to analyze the topology of **15** and **18**. In **15**, the side chain anchored to the nitrogen atom could be represented as $\text{N-C-C-C-C}=\text{C}(\text{CH}_3)_2$ (omitting methyl and vinyl groups linked to the carbon atom next to the nitrogen, which were not important in this case). The terminal C=C bond in **15** is placed topologically at the ideal distance to make an intramolecular loop and establish the π - π stacking interaction with the tetrazole moiety: C=C is separated from the nitrogen by three tetrahedral carbon atoms. In **18**, the side chain anchored to the nitrogen atom could be represented as $\text{N-C-C}=\text{C-C-C-C}=\text{C}(\text{CH}_3)_2$. In **18**, the carbon chain is longer, but it is more rigid than in **15**. The carbon chain separating the terminal double bond C(6)=C(7) from the anchor nitrogen atom is by two carbon atoms longer, but has only two tetrahedral carbon atoms: as it was discussed above, the atoms adjacent to C(2)=C(3) constitute a rigid mini-plane and render lack of flexibility in the nerol residue of **18**. This imposes restrictions on the spatial position of the remaining fragment. Indeed, the reference distances C(T)-C(6) and C(T)-C(7) in the second most stable conformer of **18** amount to 3.64 and 4.84 Å,

clearly indicating the remoteness of the tetrazole from the C=C bond. Under such circumstances, the stabilizing π - π stacking interaction cannot be established. This is demonstrated in Fig. 9. To reinforce this conclusion, it should be stated that the most stable conformer of **18** does not have the tetrazolone moiety and nerol residue in a close proximity to each other. Instead there is a "coiled" geometry having a relative proximity of C(2)=C(3) and C(6)=C(7) bonds (Fig. 10), but the stabilizing interaction of these π -systems is weaker, than that existing in **15**.

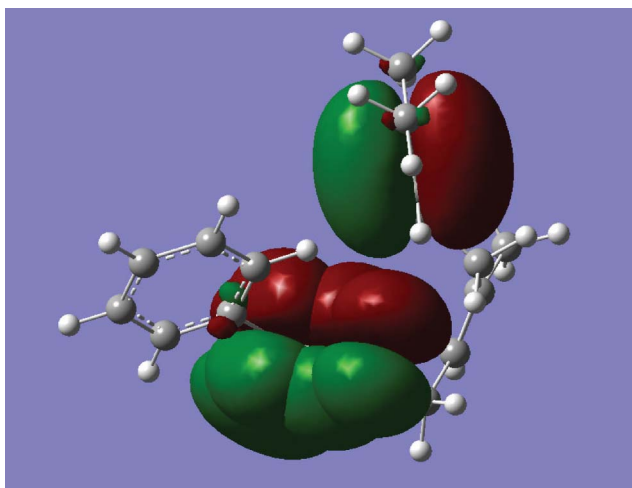


Fig. 9 Selected π -orbitals of the tetrazolone moiety and π -orbital of the terminal C=C bond of the nerol residue in the second most stable conformer of tetrazolone **18**. Note the lack of co-planarity of the two π -electron systems and the lack of orbital overlap.

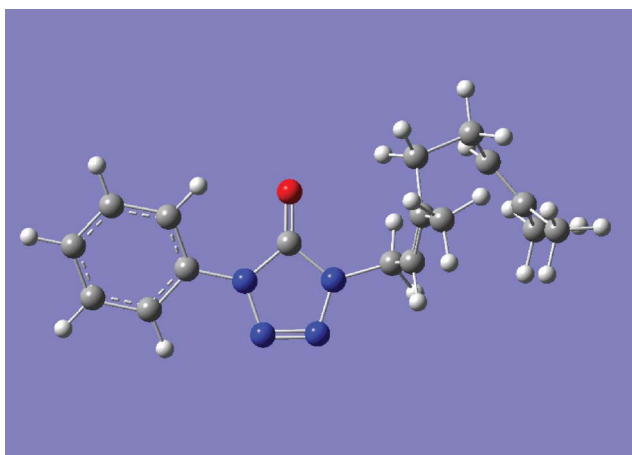


Fig. 10 Optimized MP2 geometry of the most stable conformer of tetrazolone **18**.

The above findings show clearly the importance of accounting for the non-covalent interactions in the interpretation of the conformational picture of the studied compounds. The DFT calculations failed to find minima for the structures predicted as the most stable structures at the MP2 level. This also explains why the full conformational search at the cheaper and faster theory levels, as for example semi-empirical or DFT calculations, could not be sufficient to rationalize the observations of the present study.

2.3.2. Mechanism of isomerization. In all calculations, the relative zero level of energy was chosen to be the energy of the most stable ether conformer. The calculated relative energies for the sigmatropic shifts in nerol derivative **14** are shown in the last section of each of Tables 3S and 4S, ESI,† and in Fig. 11 (energy profiles for isomerization). The calculations show that the [1,3']-sigmatropic shift is energetically more demanding as compared with the [3,3']-shift. At the DFT level of theory, the transition state for the [1,3']-shift is above 134 kJ mol⁻¹ (**TS3a**), while at the MP2 level this value increases up to above 197 kJ mol⁻¹. As observed for the sigmatropic migration of ethers **9** and **10**, the calculated barriers for the [3,3']-shifts were found to be much lower: 101 kJ mol⁻¹ (DFT) and 125 kJ mol⁻¹ (MP2) (see **TS3b** in Fig. 11). Therefore, the [3,3']-shift should dominate kinetically over the [1,3']-shift, as observed for ethers **9** and **10**.

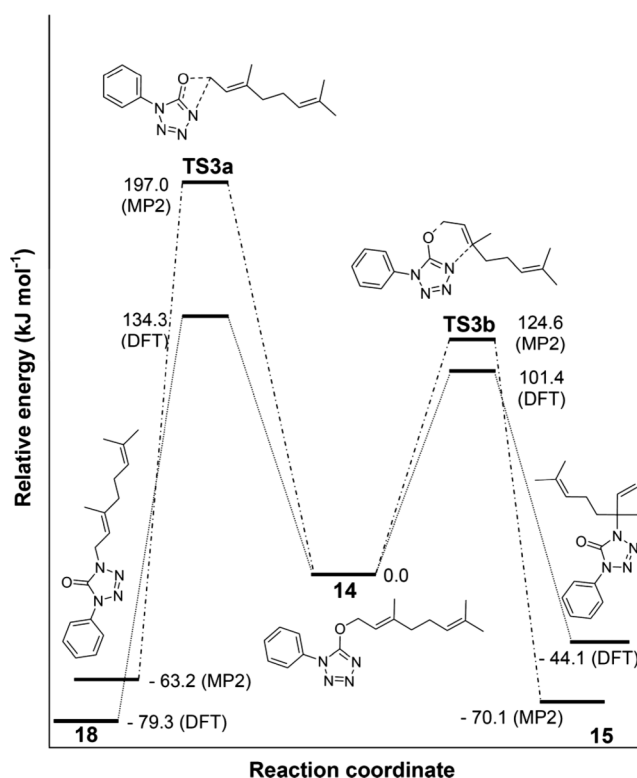
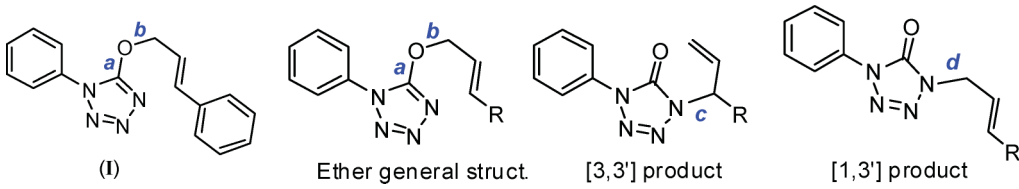


Fig. 11 Relative energies of the most stable stationary points for the thermal isomerization of (*E*)-5-(3,7-dimethylocta-2,6-dienyl)-1-phenyl-1*H*-tetrazole (**14**) into 1-(3,7-dimethylocta-1,6-dien-3-yl)-4-phenyl-1*H*-tetrazol-5(4*H*)-one (**15**) and (*E*)-1-(3,7-dimethylocta-2,6-dienyl)-4-phenyl-1*H*-tetrazol-5(4*H*)-one (**18**) calculated at the DFT(B3LYP)/6-31G(d,p) (ΔE_G) and MP2/6-31G(d,p) (ΔE_d) levels.

According to all calculations, tetrazolones formed in both processes of sigmatropic shift are more stable than the starting ether **14**. For the [1,3']-shift, the gain in stability for the most stable conformer of tetrazolone **18** is 79 kJ mol⁻¹, at the DFT level, but only 63 kJ mol⁻¹ at the MP2 level. For the [3,3']-shift, the most stable conformer of the final tetrazolone product (**15**) presents a gain in stability of 44 kJ mol⁻¹, at the DFT level, and of 70 kJ mol⁻¹ at the MP2 level. Thus, the DFT calculations (see Table 3S, ESI†) predict the product of the [3,3']-shift to be higher in energy by as

Table 5 Selected structural data obtained from X-ray crystallographic analysis and molecular orbital calculations for 1-aryl-5-allyloxytetrazoles **9**, **10**, **14** and **I** and 1-aryl-4-allyltetrazol-5-ones (**11**, **12**, and **15–18**)


Structure	Bond distances/pm				Angles/°	Method
	C– <i>a</i> –O	C– <i>b</i> –O	C– <i>c</i> –N	C– <i>d</i> –N		
9	132.7 133.5	148.5 147.9	—	—	116.3 113.9	DFT MP2
11	—	—	146.6 146.6	—	—	DFT MP2
16	—	—	—	146.6 146.6	—	DFT MP2
10	132.4 133.4	149.1 148.2	—	—	116.0 113.9	DFT MP2
12	—	—	149.8 148.3	—	—	DFT MP2
17	—	—	—	146.8 146.8	—	DFT MP2
14	132.6 133.4	147.1 146.5	—	—	116.6 113.4	DFT MP2
15	—	—	148.4 146.9	—	—	DFT MP2
18	—	—	—	146.5 145.6	—	DFT MP2
I	131.6	148.9	—	—	115.5	X-ray

much as 35 kJ mol⁻¹ as compared to the product of the [1,3']-shift but the MP2 calculations carried out for the same compounds (see Table 4S, ESI†), predict the [3,3']-shift to be lower in energy by 7 kJ mol⁻¹ as compared to the product of the [1,3']-shift (Fig. 11).

As explained above, the DFT methods revealed to be inadequate for this system, due to their incapacity for accounting for the stabilizing effect of non-covalent interactions such as π - π stacking between the heteroaromatic tetrazolyl system and the overlapping terminal double bond of the *N*-terpenyl substituent in compound **15**. On the contrary, the results obtained by MP2 methods are in keeping with the experimental data, predicting that the control over the outcome of the isomerization reaction of **14** is both kinetic (lower barriers) and thermodynamic (lower energies of the products) and that the expected product should be that corresponding to the [3,3']-shift, compound **15**. The experimental data are in agreement with this conclusion, showing that the tetrazolone adopts the structure consistent with the [3,3']-shift mechanism (¹H-NMR spectra, ESI†).

The electron-withdrawing effect of the heteroaromatic system on the ground state structures of some allylic derivatives of tetrazole has been discussed and related to observed reactivity.²² Table 5 shows selected geometric parameters for the most stable conformers of ethers **9**, **10**, and **14** and tetrazolones **11**, **12**, and **15–18**, obtained from theoretical calculations (DFT and MP2). For comparative purposes, the corresponding parameters for 5-cinnamyloxy-1-phenyl tetrazole (**I**) obtained by X-Ray crystallography, are also included. For ethers **9**, **10**, and **14**, the calculated length for C–O bond *a* is around 133 pm, and for C–O bond *b* is around 148 pm. These theoretical values are very close to those experimentally obtained for the cinnamyloxy derivative **I** (132 pm for bond *a* and 149 pm for bond *b*). Thus, due to the electron-withdrawing effect of the tetrazole ring, bond *a* exhibits a considerable degree of double bond character whereas bond *b* is longer, and weaker, than a common C–O bond in an aliphatic ether (typically 143 pm). Also, the C–O–C bond angles range from 113

to 117°, which is very close to the value experimentally obtained for ether **I** in the condensed phase (116°) and implies a significant degree of sp² character on oxygen. Thus, in the ground state, the structures of ethers **9**, **10**, and **14** are already advanced along the reaction coordinate for isomerisation, thus explaining the ease of isomerisation in these ethers.

C–N bond lengths *c*, in tetrazolones **11**, **12**, and **15**, range from 147 to 150 pm, the difference reflecting the relative bulkiness of the substituents connected to carbon. For tetrazolones **16–18**, bond lengths *d* for the less crowded C–N bonds are around 147 pm. The values for bond lengths *c* and *d* are unexceptional, indicating that the electron-withdrawing power of the tetrazole is much less effective towards the allyl group attached to nitrogen than it is when the group is attached to oxygen. This is in keeping with what has been observed from the X-ray structure of *N*-myrtenyl benzisothiazole (saccharin).²²

3. Conclusions

Mechanisms of thermal isomerization of allyl tetrazolyl ethers derived from the carbocyclic allylic alcohols cyclohex-2-enol and 3-methylcyclohex-2-enol and from the natural terpene alcohol nerol were investigated. These 1-aryl-5-allyloxytetrazoles undergo rapid isomerization to the corresponding 1-aryl-4-allyltetrazol-5-ones and the results of our investigation showed that the imidates rearrange exclusively through a [3,3']-sigmatropic migration of the allylic system from *O* to *N*, with inversion. Mechanistic proposals are based on the product analysis and extensive quantum chemical calculations at the DFT(B3LYP) and MP2 levels, on *O*-allyl and *N*-allyl isomers and on putative transition state structures for [1,3']- and [3,3']-sigmatropic migrations. The experimental observations could be only explained on the basis of the MP2/6-31G(d,p) calculations that favoured the [3,3']-sigmatropic migrations, yielding lower energies both for the transition states and for the final isomerization products. DFT

methods proved to be inadequate for these compounds, due to their poor performance on predicting and accounting for non-covalent interactions. In fact, the stabilizing effect of π - π stacking interactions established between the tetrazolyl system and the double bond of the allylic substituent appears to be instrumental in dictating the reaction pathway, accounting for the exclusive formation of the [3,3']-isomer. The observed selectivity in the synthesis of allyl tetrazolones is of great interest because these compounds may be used as starting materials in the preparation of other heterocycles, namely pyrimidinones.

4. Experimental section

4.1. Equipment and experimental conditions

All chemicals were used as purchased from Aldrich. Solvents for extraction and chromatography were of technical grade. When required, solvents were freshly distilled from appropriate drying agents before use. Analytical TLC was performed with Merck silica gel 60 F₂₅₄ plates. Melting points were recorded on a Stuart Scientific SMP3 melting point apparatus and are uncorrected. Mass spectra were obtained on a VG 7070E mass spectrometer by electron ionization (EI) or chemical ionization (CI, NH₃) at 70 eV. NMR (400 MHz) spectra were obtained on a Bruker AM-400 spectrometer using TMS as the internal reference (δ = 0.0 ppm). Elemental analyses were performed on an EA1108-Elemental Analyzer (Carlo Erba Instruments). Infrared spectra were obtained on a Bruker FTIR-TENSOR 27 spectrometer.

4.2. Synthesis of 5-allyloxytetrazoles and 4-allyltetrazol-4-ones

4.2.1. 5-(Cyclohex-2-enyloxy)-1-phenyl-1H-tetrazole (9). Cyclohex-2-enol (1.36 g; 13.9 mmol) in dry THF (30 mL) was added to a slurry of sodium hydride (55% in mineral oil; 0.65 g; 14.9 mmol) in dry THF (5 mL). When effervescence of hydrogen had ceased (30 min), 5-chloro-1-phenyl-1H-tetrazole (2.5 g; 13.9 mmol) in dry THF (20 mL) was added and the final mixture was stirred at room temperature for 3 h, when TLC analysis (EtOAc/hexane 1 : 1) indicated the absence of starting material. The solvent was removed under reduced pressure at RT to give a residue. This residue was extracted with ethyl acetate (3 \times 50 mL) and the organic extract was washed with ice water (3 \times 50 mL). The organic phase was dried (Na₂SO₄) and the filtrate evaporated to dryness to give colourless oil. Recrystallization with ethanol gave the 5-(cyclohex-2-enyloxy)-1-phenyl-1H-tetrazole as white crystals (2.1 g; 61% yield), mp 60–62 °C. IR ν_{max} : 2927, 1591, 1549, 1504, 1457, 910 cm⁻¹; ¹H NMR (400 MHz, CD₃OD): δ 1.66–1.83 (2H, m, -CH₂-), 2.04–2.18 (4H, m, -CH₂-), 5.47–5.48 (1H, m, CH-O-), 5.98, 6.00 (1H, d, -CH=), 6.09–6.13 (1H, m, =CH-), 7.47–7.51 (1H, t, ArH), 7.54–7.58 (2H, t, ArH), 7.70–7.72 (2H, d, ArH); ¹³C NMR (100 MHz, CD₃OD): δ_{c} 18.06, 24.64, 27.87, 78.52, 121.85, 123.44, 128.98, 129.44, 133.47, 134.91, 159.85 MS (EI), m/z 242 [M]⁺.

4.2.2. 4-(Cyclohex-2-enyl)-1-phenyl-1H-tetrazol-5(4H)-one (11). A neat sample of 5-(cyclohex-2-enyloxy)-1-phenyl-1H-tetrazole (1.0 g; 4.1 mmol) was heated at 40 °C for 2 h to give 1-(cyclohex-2-enyl)-4-phenyl-1H-tetrazol-5(4H)-one as yellow oil (quantitative yield). IR ν_{max} : 2927, 1724, 1595, 1552, 1504, 1459, 904 cm⁻¹; ¹H NMR (400 MHz, CD₃OD): δ 1.71–2.23 (6H, m,

-CH₂-), 4.88–4.91 (1H, m, CH-N), 5.71–5.74 (1H, d, -CH=), 6.08–6.10 (1H, m =CH-), 7.39–7.42 (1H, t, ArH), 7.50–7.54 (2H, t, ArH), 7.87–7.89 (2H, d, ArH); ¹³C NMR (100 MHz, CDCl₃): δ_{c} 20.14, 24.78, 28.70, 52.03, 77.14, 77.45, 77.77, 119.71, 124.31, 127.98, 129.73, 133.45, 135.19; MS (EI), m/z 243 [M+H]⁺.

4.2.3. 5-(3-Methylcyclohex-2-enyloxy)-1-phenyl-1H-tetrazole (10). The synthesis of tetrazolyl ether **10** was attempted using several sets of experimental conditions. However, the desired ether could never be recovered. Instead, the product of its isomerization, 4-allyltetrazol-5-one (**12**) was isolated in all cases. A general procedure for the synthesis of this compound is described.

4.2.4. 4-(3-Methylcyclohex-2-enyl)-1-phenyl-1H-tetrazol-5(4H)-one (12). 3-Methyl-cyclohex-2-enol (0.62 g; 5.54 mmol) in dry THF (30 mL) was added to slurry of sodium hydride (55% in mineral oil; 0.32 g; 7.4 mmol) in dry THF (5 mL). When effervescence of hydrogen had ceased (20 min), 5-chloro-1-phenyl-1H-tetrazole (1.0 g; 5.54 mmol) in dry THF (10 mL) was added and the mixture was stirred at \approx 10 °C for 4 h until analysis by TLC (AcOEt/hexane 1 : 1) indicated the absence of starting material. The solvent was removed under reduced pressure at RT to give a residue. This residue was extracted with ethyl acetate (3 \times 50 mL) and the organic extract was washed with ice water (3 \times 50 mL). The organic extract was dried (Na₂SO₄) and the filtrate evaporated to dryness to give the 4-(3-methylcyclohex-2-enyl)-1-phenyl-1H-tetrazol-5(4H)-one as light yellow oil (1.1 g; 71% yield). IR ν_{max} : 2927, 1721, 1596, 1504, 1460, 1367, 1095, 904 cm⁻¹; ¹H NMR (400 MHz, CD₃OD): δ 1.69 (3H, s, CH₃), 1.79–1.86 (4H, m, -CH₂CH₂-), 2.09–2.11 (2H, m, CH₂), 5.97–6.03 (2H, m, CH=CH), 7.38–7.42 (1H, t, ArH), 7.50–7.54 (2H, t, ArH), 7.85–7.87 (2H, d, ArH); ¹³C NMR (100 MHz, CD₃OD): δ_{c} 18.34, 24.21, 25.29, 32.78, 60.16, 119.63, 127.59, 128.15, 129.05, 130.50, 134.59, 148.71; MS (EI), m/z 257 [M]⁺.

4.2.5. (E)-5-(3,7-Dimethylocta-2,6-dienyloxy)-1-phenyl-1H-tetrazole (14). The synthesis of tetrazolyl ether **14** was attempted using several sets of experimental conditions. However, due to an easy and fast isomerisation of ether **14** only a mixture of this ether and its *N*-allyl isomer **15** could be characterized. ¹H-NMR signals are easily distinguishable by their integration ratio. The signal chosen for the integration ratio of these two compounds was at 7.70–7.72 (two protons from ether **14**). The integral value 0.4 was assigned as one hydrogen is present in the *N*-allyl isomer. A general procedure for the synthesis of this compound is described.

(*E*)-3,7-Dimethylocta-2,6-dien-1-ol (Nerol; 2.15 g; 13.9 mmol) in dry THF (20 mL) was added to a slurry of sodium hydride (60% in mineral oil; 0.60 g; 14.6 mmol) in dry THF (20 mL). When effervescence of hydrogen had ceased (30 min.), 5-chloro-1-phenyl-1H-tetrazole (2.5 g; 13.9 mmol) in dry THF (20 mL) was added and the reaction was stirred at \approx 10 °C for 12 h. The reaction was monitored by TLC using a mixture of toluene/acetone (5 : 1) as eluent. The solvent was removed under reduced pressure at RT to give a residue. This residue was extracted with ethyl acetate (3 \times 50 mL) and the organic extract was washed with ice water (3 \times 50 mL). The organic phase was dried (Na₂SO₄) and evaporated to dryness to give a yellow solid. Recrystallization with ethanol gave the required product as white crystals (1.0 g; 24% yield), mp 43–45 °C. IR ν_{max} : 2967, 2912, 2858, 1592, 1570, 1506, 1460, 1443, 939; ¹H NMR (400 MHz, CD₃OD): δ 1.56 (3H, s, CH₃), 1.60 (3H,

s, CH₃), 1.81 (3H, s, CH₃), 2.09–2.14 (2H, q, CH₂), 2.21–2.25 (2H, t, CH₂), 5.09, 5.10 (3H, d, =CH–, CH₂), 5.58–5.61 (1H, t, =CH–), 7.48–7.52 (1H, m, ArH), 7.55–7.58 (2H, t, ArH), 7.70, 7.72 (2H, d, ArH);

4.2.6. 1-(3,7-Dimethylocta-1,6-dien-3-yl)-4-phenyl-1H-tetrazol-5(4H)-one (15). The solution remaining from the recrystallization of ether **14** was evaporated under reduced pressure, to afford the required product as yellow oil (1.6 g, 36% yield).

A neat sample of (*E*)-5-(3,7-dimethylocta-2,6-dienyloxy)-1-phenyl-1H-tetrazole (0.8 g; 2.7 mmol) was heated at 40 °C for 1 h to give 1-(cyclohex-2-enyl)-4-phenyl-1H-tetrazol-5(4H)-one as yellow oil (quantitative yield). IR ν_{max} : 1725, 1598, 1560, 1502, 1376, 757 cm⁻¹; ¹H NMR (400 MHz, CDCl₃): δ 1.54 (3H, s, CH₃), 1.57 (3H, s, CH₃), 1.77 (3H, s, CH₃), 1.98–2.37 (4H, m, –CH₂CH₂–), 5.01–5.07 (1H, t, =CH–), 5.16–5.25 (2H, m, =CH₂), 6.23–6.30 (1H, m, =CH–), 7.36–7.40 (1H, t, ArH), 7.48–7.52 (2H, t, ArH), 7.85, 7.87 (2H, d, ArH); ¹³C NMR (100 MHz, CD₃OD): δ_{c} 16.37, 21.69, 22.19, 24.54, 36.97, 64.95, 113.63, 119.38, 122.75, 127.53, 129.03, 131.75, 134.55, 139.51, 148.76; MS (EI), *m/z* 299 [M+H]⁺; Anal. Calcd for C₁₇H₂₂N₄O: C, 68.43; H, 7.43; N, 18.78%. Found: C, 68.22; H, 7.75; N, 18.30%.

4.3. Computational details

For all considered systems, all the calculations were carried out using the Gaussian 03 program package.³¹ At the DFT(B3LYP) level of theory^{32,33} with the standard 6-31G(d,p) basis set,³⁴ the geometries of the investigated molecules were fully optimized and the harmonic vibrational frequencies were calculated. The nature of the obtained stationary points was checked through the analysis of the corresponding Hessian matrices. Absence of imaginary frequencies indicated that they correspond to true minima. This also enabled the determination of thermodynamic quantities such as zero-point-corrected vibrational energy and free energy at 298.15 K. All relevant barriers to intramolecular rearrangements were calculated using either the QST2 or QST3 variety of the synchronous transit-guided quasi-Newton (STQN) method.^{35,36} All transition states were characterized as first-order saddle points by the presence of one imaginary frequency, as revealed by analysis of the corresponding Hessian matrices and visualization of the corresponding vibrational mode graphically. Natural bond orbital (NBO) analysis was performed using NBO 3, as implemented in Gaussian 03.

The full geometry optimizations were also carried out at the MP2 level of theory^{37–39} with the same 6-31G(d,p) basis set as used in the DFT calculations. The large size of the studied molecules did not allow analytical calculation of the MP2 vibrational frequencies, due to the limitations of the 32-bit version of Gaussian 03 for Windows. Their characterization as minima or saddle points was concluded on the basis of geometrical resemblance with the similar structures obtained at the DFT level of theory and also based on the absence of the lower-energy structures after applying optimization with the “tight” criteria and without symmetry restriction. For a few most important geometries (the most stable conformers of **10**, **12**, **17**, **TS2a** and **TS2b**), the vibrational MP2 characterization was carried out numerically, at a very high computational cost, and confirmed the general conclusions.

Acknowledgements

The authors acknowledge Fundação para a Ciência e Tecnologia (FCT) and FEDER [Project PTDC/QUI/67674/2006 and grants BD/17945/2004 and BPD/43853/2008], for financial support.

References

- S. C. S. Bugalho, E. M. S. Mações, M. L. S. Cristiano and R. Fausto, *Phys. Chem. Chem. Phys.*, 2001, **3**, 3541.
- T. Mavroumoustakos, A. Kolocouris, M. Zervou, P. Roumelioti, J. Matsoukas and R. Weisemann, *J. Med. Chem.*, 1999, **42**, 1714.
- J. H. Toney, P. M. D. Fitzgerald, N. Grover-Sharma, S. H. Olson, W. J. May, J. G. Sundelof, D. E. Vanderwall, K. A. Cleary, S. K. Grant, J. K. Wu, J. W. Kozarich, D. L. Pompliano and G. G. Hammond, *Chem. Biol.*, 1998, **5**, 185.
- Y. Hashimoto, R. Ohashi, Y. Kurosawa, K. Minami, H. Kaji, K. Hayashida, H. Narita and S. Murata, *J. Cardiovasc. Pharmacol.*, 1998, **31**, 568.
- A. Desarro, D. Ammendola, M. Zappala, S. Grasso and G. B. Desarro, *Antimicrob. Agents Chemother.*, 1995, **39**, 232.
- A. D. Abell and G. J. Foulds, *J. Chem. Soc., Perkin Trans. 1*, 1997, 2475.
- Y. Tamura, F. Watanabe, T. Nakatani, K. Yasui, M. Fujii, T. Komurasaki, H. Tsuzuki, R. Maekawa, T. Yoshioka, K. Kawada, K. Sugita and M. Ohtani, *J. Med. Chem.*, 1998, **41**, 640.
- G. Sandmann, C. Schneider and P. Boger, *Z. Naturforsch. C*, 1996, **51**, 534.
- G. I. Koldobskii, V. A. Ostrovskii and V. S. Poplavskii, *Khim. Geterosikl. Soedin.*, 1981, **10**, 1299.
- R. A. Abramovitch, C. I. Azogu, I. T. McMaster and D. P. Vanderpool, *J. Org. Chem.*, 1978, **43**, 1218.
- L. M. T. Frija, R. Fausto, R. M. S. Loureiro and M. L. S. Cristiano, *J. Mol. Catal. A: Chem.*, 2009, **305**, 142.
- L. M. T. Frija, I. V. Khmelinskii and M. L. S. Cristiano, *Tetrahedron Lett.*, 2005, **46**, 6757.
- L. M. T. Frija, I. V. Khmelinskii and M. L. S. Cristiano, *J. Org. Chem.*, 2006, **71**, 3583.
- L. M. T. Frija, I. V. Khmelinskii, C. Serpa, I. D. Reva, R. Fausto and M. L. S. Cristiano, *Org. Biomol. Chem.*, 2008, **6**, 1046.
- L. M. T. Frija, A. Ismael and M. L. S. Cristiano, *Molecules*, 2010, **15**, 3757.
- R. A. W. Johnstone, A. H. Wilby and I. D. Entwistle, *Chem. Rev.*, 1985, **85**, 129.
- M. L. S. Cristiano, R. A. W. Johnstone and P. J. Price, *J. Chem. Soc., Perkin Trans. 1*, 1996, 1453.
- N. C. P. Araújo, A. F. Brigas, M. L. S. Cristiano, L. M. T. Frija, E. M. O. Guimarães and R. M. S. Loureiro, *J. Mol. Catal. A: Chem.*, 2004, **215**, 113.
- L. M. T. Frija, M. L. S. Cristiano, E. M. O. Guimarães, N. C. Martins, R. M. S. Loureiro and J. Bickley, *J. Mol. Catal. A: Chem.*, 2005, **242**, 241.
- S. C. S. Bugalho, L. Lapinski, M. L. S. Cristiano, L. M. T. Frija and R. Fausto, *Vibrat. Spectrosc.*, 2002, 3541.
- J. V. Barkley, M. L. S. Cristiano, R. A. W. Johnstone and R. M. S. Loureiro, *Acta Crystallogr., Sect. C: Cryst. Struct. Commun.*, 1997, **53**, 383.
- N. C. P. Araújo, P. M. M. Barroca, J. F. Bickley, A. F. Brigas, M. L. S. Cristiano, R. A. W. Johnstone, R. M. S. Loureiro and P. C. A. Pena, *J. Chem. Soc., Perkin Trans. 1*, 2002, 1213.
- M. L. S. Cristiano, A. F. Brigas, R. A. W. Johnstone, R. M. S. Loureiro and P. C. A. Pena, *J. Chem. Res. (S)*, 1999, 704.
- A. Gómez-Zavaglia, A. Kaczor, R. Almeida, M. L. S. Cristiano, M. E. S. Eusébio, T. M. R. Maria, P. Mobilis and R. Fausto, *J. Phys. Chem. A*, 2009, **113**, 3517.
- M. L. S. Cristiano and R. A. W. Johnstone, *J. Chem. Soc., Perkin Trans. 2*, 1997, 489.
- M. L. S. Cristiano and R. A. W. Johnstone, *J. Chem. Res. (S)*, 1997, 164.
- I. Dąbkowska, P. Jurečka and P. Hobza, *J. Chem. Phys.*, 2005, **122**, 204322.
- W. McCarthy, A. M. Plokhotnichenko, E. D. Radchenko, J. Smets, D. M. A. Smith, S. G. Stepanian and L. Adamowicz, *J. Phys. Chem. A*, 1997, **101**, 7208.

- 29 J. Gu, J. Wang, J. Leszczynski, Y. Xie and H. F. Schaefer III, *Chem. Phys. Lett.*, 2008, **459**, 164.
- 30 Brijesh Kumar Mishra, J. Samuel Arey and N. Sathyamurthy, *J. Phys. Chem. A*, 2010, **114**, 9606.
- 31 M. J. Frisch, G. W. Trucks, H. B. Schlegel, G. E. Scuseria, M. A. Robb, J. R. Cheeseman, J. A. Montgomery, Jr., T. Vreven, K. N. Kudin, J. C. Burant, J. M. Millam, S. S. Iyengar, J. Tomasi, V. Barone, B. Mennucci, M. Cossi, G. Scalmani, N. Rega, G. A. Petersson, H. Nakatsuji, M. Hada, M. Ehara, K. Toyota, R. Fukuda, J. Hasegawa, M. Ishida, T. Nakajima, Y. Honda, O. Kitao, H. Nakai, M. Klene, X. Li, J. E. Knox, H. P. Hratchian, J. B. Cross, V. Bakken, C. Adamo, J. Jaramillo, R. Gomperts, R. E. Stratmann, O. Yazyev, A. J. Austin, R. Cammi, C. Pomelli, J. Ochterski, P. Y. Ayala, K. Morokuma, G. A. Voth, P. Salvador, J. J. Dannenberg, V. G. Zakrzewski, S. Dapprich, A. D. Daniels, M. C. Strain, O. Farkas, D. K. Malick, A. D. Rabuck, K. Raghavachari, J. B. Foresman, J. V. Ortiz, Q. Cui, A. G. Baboul, S. Clifford, J. Cioslowski, B. B. Stefanov, G. Liu, A. Liashenko, P. Piskorz, I. Komaromi, R. L. Martin, D. J. Fox, T. Keith, M. A. Al-Laham, C. Y. Peng, A. Nanayakkara, M. Challacombe, P. M. W. Gill, B. G. Johnson, W. Chen, M. W. Wong, C. Gonzalez and J. A. Pople, *GAUSSIAN 03 (Revision C.02)*, Gaussian, Inc., Wallingford, CT, 2004.
- 32 A. D. Becke, *Phys. Rev. A: At., Mol., Opt. Phys.*, 1988, **38**, 3098.
- 33 C. T. Lee, W. T. Yang and R. G. Parr, *Phys. Rev. B*, 1988, **37**, 785.
- 34 M. Frisch, M. Head-Gordon and J. Pople, *Chem. Phys. Lett.*, 1990, **166**, 281.
- 35 C. Peng, C. Y. Peng, P. Y. Ayala, H. B. Schlegel and M. J. Frisch, *J. Comput. Chem.*, 1996, **17**, 49.
- 36 C. Peng and H. B. Schlegel, *Isr. J. Chem.*, 1994, **33**, 449.
- 37 H. Basch and W. J. Stevens, *Chem. Phys. Lett.*, 1990, **169**, 275.
- 38 L. F. Pacios, *Chem. Phys. Lett.*, 1990, **169**, 281.
- 39 M. Head-Gordon and T. Head-Gordon, *Chem. Phys. Lett.*, 1994, **220**, 122.